Arab J Geosci (2015) 8:8835–8851
DOI 10.1007/s12517-015-1799-2

ORIGINAL PAPER

Hydrochemistry, evolution, and origin of brines in supratidal saline pans, south Jeddah, Red Sea coast, Saudi Arabia

Rushdi J. Taj · Mahmoud A. Aref

Received: 30 June 2014 / Accepted: 20 January 2015 / Published online: 17 February 2015

Abstract The supratidal, saline pans and surrounding wet sabkha area, south Jeddah, Saudi Arabia, have seawater seepages with a salinity of 40‰ that increases to 80–140 and 220–375‰ during deposition of gypsum and halite, respectively. The concentration order of the dominant cations and anions in the saline pans is sodium (Na^+)>magnesium (Mg^{2+})>potassium (K^+)>calcium (Ca^{2+}) and chloride (Cl^-)>sulfate ions (SO_4^{2-})>bicarbonate ions (HCO_3^-), respectively. The dominant brine type is Mg and sodium chloride. Correlations of the various ions in the saline pans indicate positive relations between Na^+ and Cl^-, Na^+ and total dissolved solids (TDS), and Cl^- and TDS due to halite precipitation at a high salinity value. Negative correlations between Ca^{2+} and SO_4^{2-} and between Ca^{2+} and HCO_3^- are related to the reduction of SO_4^{2-} and oxidation of organic matter by sulfate-reducing bacteria, which is confirmed also by the positive correlation of HCO_3^- and alkalinity. The high Mg/Ca ratio is related to the enrichment of the brine with bittern salts such as $MgCl_2$ and KCl. The chemical data of the brines indicate their source from recent and old marine waters of $MgCl_2$ and $CaCl_2$ characters. The contribution of meteoric water has a minor effect on the composition of the brine in the saline pans.

Keywords Brine chemistry · Evolution · Genesis · Saline pans · Seawater seepage · Saudi Arabia

R. J. Taj · M. A. Aref (✉)
Department of Petroleum Geology and Sedimentology, Faculty of Earth Sciences, King Abdulaziz University, Jeddah, Saudi Arabia
e-mail: m1aref@yahoo.com

M. A. Aref
Geology Department, Faculty of Science, Cairo University, Giza, Egypt

Introduction

Saline pans are enclosed or mostly enclosed water bodies floored with layered evaporite minerals in continental and marginal marine settings in arid or semiarid regions (Lowenstein and Hardie 1985; Macumber 1991). Marginal marine pans are typically hypersaline with water salinities typically in excess of 50‰ and mostly exhibit a marine-like chemical character in which sodium (Na^+) and chloride (Cl^-) strongly dominate (Herczeg et al. 2001). High rates of evaporation are the primary control on the chemical character even though a broad range of secondary processes can significantly affect the evaporative pathways and dictate the ultimate water chemistry (Radke et al. 2002). These processes include mineral dissolution, seawater intrusion, cation exchange reactions, sulfate reduction, mixing, brine reflux, mineral precipitation, and recycling of soluble salts within the pans (Radke and Howard 2007).

The Red Sea coastal plain of Saudi Arabia contains a series of isolated coastal lagoons, saline pans, and coastal sabkhas from Ummlajj in the north to Jizan in the south. Most studies carried out on these lagoons were concerned with their pollution from sewage, hydrography and water circulation, flushing time, diagenesis of sediments, microfossils, geochemistry, and environmental characteristics (El-Rayis and Moammar 1998; Basaham 1998; El Sayed 2002; Al-Washmi 2003; Turki 2007; Turki and Mudarris 2008; Al-Barakati 2009, 2011). Water and sediment chemistry of the eastern Red Sea supratidal sabkhas was the interest of some workers (e.g., Bahafzullah et al. 1993; Basyoni 1997; Sabtan et al. 1997; Sabtan and Shehata 2003; Banat et al. 2005), whereas other sabkhas in Saudi Arabia were studied by Alsaaran (2008), Basyoni and Mousa (2009), Al-Harbi et al. (2010), and Al-Shaibani (2013). Saline pans in the Red Sea coast of Saudi Arabia have

received little attention and remain poorly understood. However, in Makkah area, west of the studied saline pans, the hydrogeological and hydrochemical characteristics of shallow and deep aquifers were concerned with groundwater conditions, aquifer characteristics, groundwater quality, and hydrochemistry of the major ions (e.g., Alyamani et al. 1996; Alyamani 1999, 2007; Al-Ahmadi 2013; Sharaf 2013).

The Şarūm saline pans are developed recently over sabkha and lagoonal sediments due to artificial construction of an asphaltic road in the last 30 years which allowed their restriction and deposition of halite and gypsum on the floor of the pans. The peculiarity of the Şarūm saline pans is their elevated salinities from 80 to 375‰, which are higher than the salinity of most evaporite basins in the eastern Red Sea coast. The purpose of this paper is to delineate the chemical composition and origin of the brines in the saline pans. The paper describes also the evolution of the brines from seepage seawater to microbial mats—carbonate, gypsum, and halite-saturated brine. The results of this paper can be used to interpret the chemical evolution and origin of brines of similar ancient, saline pan evaporite deposits.

Methodology

This work is based on several field trips in different seasons and weather condition to the studied saline pans during the period from April 2010 through May 2013. In each trip, the salinity and temperature in the pans were measured. The salinity was determined by hydrometer glasses taking into account the measuring of standard seawater. The hydrometer measures the mass % NaCl in the brine up to 250‰. Temperatures were measured at the surface by mercury thermometer ranging from 0 to 100 °C in 0.1 °C divisions. The density of the brine samples was measured by using two portable hydrometer glasses: the first measures density from 1.00 to 1.10 g/cm^3, and the second measures density from 1.10 to 1.2 g/cm^3. Major chemical analysis for 24 water and brine samples (Fig. 1c) was made at the Geochemistry Lab, Department of Mineral Resources and Rocks, Faculty of Earth Sciences, King Abdulaziz University, following the procedures given in the American Pubic Heath Association (APHA 2005). The chemical analyses were carried out for the major cations Na^+, potassium (K^+), calcium (Ca^{2+}), and magnesium (Mg^{2+}) and the major anions bicarbonate ions (HCO_3^-), carbonate ions (CO_3^{2-}), sulfate ions (SO_4^{2-}), and Cl^-. Total dissolved solids (TDS) were measured by sample evaporation technique. Ca^{2+} and Mg^{2+} are determined by complexiметric titration using standard EDTA solution. Cl^- is determined by standard (0.05 N) $AgNO_3$ titration. HCO_3^- are determined by titration with standard (0.1 N) HCl. Na^+ and K^+ are measured by flame photometry. SO_4^{2-} are determined colorimetrically using the spectrophotometer technique. The analytical precision of the ions is determined by calculating the absolute error in ionic balance in terms of equivalents per milligram (meq/l), which is found in all samples within a standard limit of ±5 %. All concentration values were expressed in milligram per liter (mg/l) unless otherwise indicated (Table 1). The chemical data were displayed in graphical forms of the Piper trilinear and Sulin diagrams to delineate the composition and origin of the brines in the saline pans.

Study area

Şarūm area is located in the Makkah quadrangle that constitutes a part of the western Arabian Shield, and is covered from east to west by (1) the Red Sea hills and pediments of the Neoproterozoic basement rocks (diorites, granodiorites, granites, andesite, dacite, and volcaniclastics), (2) the coastal hills and pediments of the Tertiary sedimentary rocks (Shumaysi, Usfan, and Hadat Ash-Sham formations) that are covered by basaltic lavas, and (3) the coastal plain Holocene marine sediments, wadi alluvium, sabkha deposits, and the aeolian sands (Moore and Al-Rehaili 1989; Spencer and Vincent 1984; Qari 2009).

The Şarūm saline pans are located in the Red Sea coastal plain, south of Jeddah city 42 km, between latitudes 21° 07′ 30″ and 21° 11′ 06″ N and longitudes 39° 09′ 54″ and 39° 12′ 03″ E (Fig. 1a). Two saline pans existed without surface connection with the Red Sea water. They occupy topographic depressions below sea level, where seawater seepage through beach sands, bioclasts, and coral rubbles was observed through numerous seepage holes. The northern is an ephemeral halite pan which is floored with halite crusts during the summer months. It has a length of 1 km, a width of 800 m, and a water depth less than 50 cm. The southern is a permanent gypsum pan, where gypsum and microbial mats are dominant on its floor. It has a length of 3 km, width that ranges from 30 to 1500 m, and a water depth less than 150 cm. The southwestern margin of the gypsum pan is close to the Red Sea coast, where a better communication is achieved through numerous seepage points.

The northern and southern saline pans of Şarūm area are formerly a supratidal sabkha and a coastal lagoon (Fig. 1b). The latter is connected with the Red Sea via a narrow, inlet and a narrow, shallow tidal creek that is closed by artificial alluvium due to road construction of the main Red Sea road of Jeddah–Jizan in the last 30 years. The Şarūm pans are considered as a former backreef lagoon. Some of their western and eastern sides are bordered by old, raised coral reef terraces, probably of Pleistocene age (Skipwith 1973; Al-Sayari and Zotl 1978; Bahafzallah and El-Askary 1981; El-Sabrouti

1983; Al-Washmi 1999; Mandurah and Aref 2012) with elevations ranging from 1 to 2 m a.s.l. The other sides of the lagoon are bordered by a low land (0.5–1 m a.s.l.) that is composed of sand-sized alluvium and sabkha. The area is developed rapidly to the present morphology due to restriction of the inflowing water.

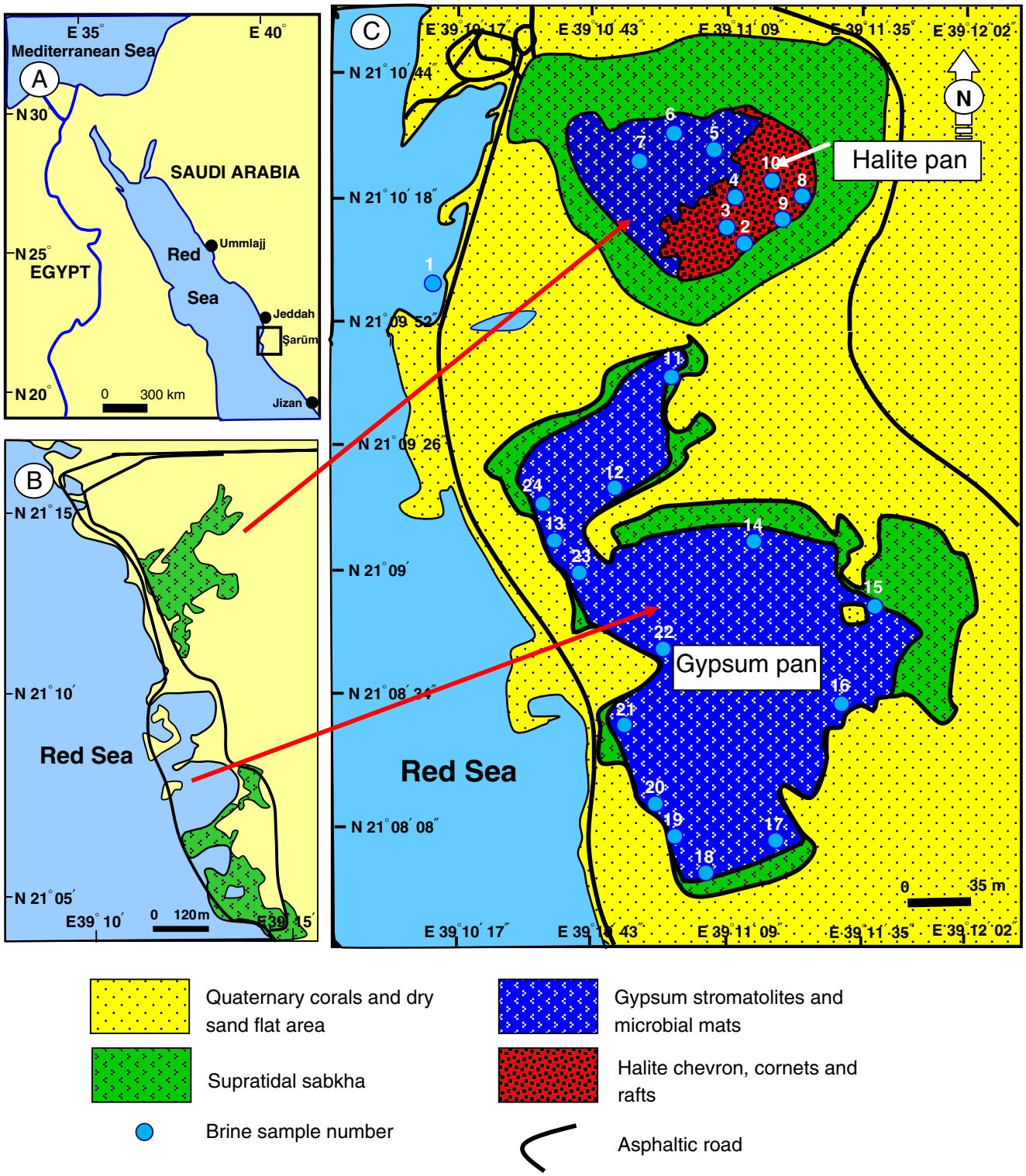

Fig. 1 Location and surface sediments of Şarūm area. **a** Location of Şarūm area south of Jeddah, Red Sea coast, Saudi Arabia. **b** Paleogeographic map of Şarūm area showing that the southern gypsum pan was a part of the sea, and the northern halite pan was a former supratidal sabkha (data from Moore and Al-Rehaili 1989). **c** Surface sediments of the saline pans of Şarūm and their surroundings

Table 1 Concentration values (mg/l) of the major cations, anions, alkalinity and TDS, Mg/Ca, and brine types in the halite pan and gypsum pan, Şarūm area

Sample number	Units	Ca^{2+}	Mg^{2+}	Na^{+}	K^{+}	SO_4^{-}	CO_3^{-}	HCO_3^{-}	Cl^{-}	Alkalinity	TDS	Mg/Ca	Brine type
Halite pan													
1	mg/l	480.96	1507.84	4800	400	336.2	90	143.3	14,215.5	192.654	29,145	3.135	Ca, Mg, sodium chloride
	epm	24	124.03	208.8	10.22	7	3	2.34	401.02				
2	mg/l	260.52	16,026.88	51,400	6100	11,623.44	0	427	211,226	350.28	359,560	61.52	Mg, sodium chloride
	epm	13	1318.37	2235.9	155.97	242	0	6.99	5958.685				
3	mg/l	641.28	7782.4	49,400	2400	39,817.5	0	244	202,351	200.16	321,204	12.14	Mg, sodium, SO_4, chloride
	epm	32	640.18	2148.9	61.36	829	0	3.99	5708.32				
4	mg/l	300.6	14,932.48	56,000	4600	5907.78	0	307	209,452	250.2	356,232	49.67	Mg, sodium chloride
	epm	15	1228.34	2436	117.62	123	0	5.03	5908.64				
5	mg/l	525.04	10,017.41	58,200	4400	1825.2	0	244	124,275	200.16	217,235	19.08	Mg, sodium chloride
	epm	26.2	824.03	2531.7	112.50	38	0	4	3505.8				
6	mg/l	921.84	7441.92	34,804	2404	1489	0	152.5	76,448.8	125.1	150,380	8.02	Mg, sodium chloride
	epm	46	612.17	1513.97	61.47	31	0	2.5	2156.62				
7	mg/l	200.4	29,208.32	41,600	8800	2833.8	0	549	15,2726.8	450.36	293,679	145.75	K, Na, magnesium chloride
	epm	10	2402.67	1809.6	225.02	59	0	9	4308.423				
8	mg/l	100.2	40,748.16	25,200	10,800	4226.7	0	732	15,997.5	600.48	375,023	406.67	K, Na, magnesium chloride
	epm	5	3351.94	1096.2	276.15	88	0	12	4513.53				
9	mg/l	521.04	11,089.92	34,800	2800	1248.8	0	305	92,454.7	250.2	227,954	21.28	Mg, sodium chloride
	epm	26	912.25	1513.8	71.59	26	0	5	2608.148				
10	mg/l	120.24	31,567.36	45,600	7600	2161.4	0	671	162,453.4	550.44	352,381	262.54	Na, magnesium chloride
	epm	6	2596.73	1983.6	149.33	45	0	11	4582.2				
Gypsum pan													
11	mg/l	1607.20	7390.84	40,000	2020	1441	240	61.61	88,984	250.7004	188,967	4.6	K, Na, magnesium chloride
	epm	80.2	607.97	1740	51.65	30	8	1.009	2510.24				
12	mg/l	801.17	7052.8	38,800	2200	1296.8	120.6	139.995	78,196.4	215.42	125,340	8.8	Mg, sodium chloride
	epm	44	580.16	1687.8	56.25	27	2.4	2.294	2205.92				
13	mg/l	1082.16	7417.6	36,000	2204	1200.7	120	137.25	76,425	212.67	145,763	6.85	Mg, sodium chloride
	epm	54	610.17	1566	56.356	25	4	2.249	2155.95				
14	mg/l	1603.2	3672.32	16,800	600	1056.7	0	152.805	36,416.2	125.35	89,730	2.29	Ca, Mg, sodium chloride
	epm	80	302.08	730.8	15.342	22	0	2.5	1027.3				
15	mg/l	1723.44	4328.96	29,200	602	768.5	0	219.6	56,831	180.144	113,631	2.51	Ca, Mg, sodium chloride
	epm	86	356.1	1270.2	15.39	16	0	3.6	1603.2				
16	mg/l	1162.32	7393.28	26,400	1000	2161.4	180.66	200.96	60,404.1	247.97	122,323	6.36	Mg, sodium chloride
	epm	58	608.17	1148.4	25.57	15	6.0214	3.294	1704				
17	mg/l	1242.48	7466.24	32,000	2000	1633	240.75	39.284	79,978	232.986	167,383	6.0	Mg, sodium chloride
	epm	62	614.17	1392	51.14	34	8.023	0.644	2256.18				
18	mg/l	889.77	2816.25	13,000	604	432.3	108	36.6	34,803.3	120.096	69,600	3.17	Ca, Mg, sodium chloride
	epm	44.4	231.66	565.5	15.44	9	3.6	0.6	981.8				
19	mg/l	1162.32	7672.96	37,400	2400	624.4	241.2	63.44	79,965.6	253.202	149,402	6.6	Mg, sodium chloride

Table 1 (continued)

Sample number	Units	Ca^{2+}	Mg^{2+}	Na^{+}	K^{+}	SO_4^{-}	CO_3^{-}	HCO_3^{-}	Cl^{-}	Alkalinity	TDS	Mg/Ca	Brine type
	epm	58	613.177	1626.9	61.368	13	8.039	1.04	2255.83				
20	mg/l	1174.34	7580.54	40,020	2402	1344.8	180	122	88,826.6	250.2	222,000	6.46	Mg, sodium chloride
	epm	58.6	623.57	1740.87	61.42	28	6	2	2505.8				
21	mg/l	1042.08	7758.05	34,802	2202	1104.7	180.6	122.305	76,400.2	250.95	131,752	7.45	Mg, sodium chloride
	epm	52	638.18	1513.887	56.305	23	6.019	2.004	2155.25				
22	mg/l	320.64	2979.2	16,000	500	4082.6	0	183	40,825	150.12	80,582	9.29	Mg, sodium, SO_4, chloride
	epm	16	245.689	696	12.785	85	0	2.99937	1151.67				
23	mg/l	701.4	8049.92	40,200	2200	4226.705	0	305	117,150	250.7	237,116	11.48	Mg, sodium chloride
	epm	35	662.18	1748.7	56.254	88	0	4.998	3304.8				
24	mg/l	1042.08	7843.2	34,700	1900	41,114.3	0	311	145,550	253.4	230,162	7.53	Mg, sodium, SO_4, chloride
	epm	52	645.18	1509.45	48.583	856	0	5.097	4105.96				

Climate and hydrography

The climate of Jeddah City is a hot arid desert type, with scarce rainfall in the spring season. The maximum temperature varies between 35.5 and 37.6 °C and the minimum temperature varies between 20.9 and 25.3 °C. The maximum humidity ranges between 78.6 and 84.6 % and minimum humidity ranges between 14.6 and 17.0 % (MAW 2003). The mean evaporation ranges between 10.0 and 12.0 mm/day, and the mean rainfall varies between 1.1 and 7.3 mm (MAW 2003). The precipitation rate is about 55 mm/year. The wind is mostly north to north-northwest throughout the year (Patzert 1974). Evaporation in the Red Sea is 2.04 m/year (Al-Subhi 2012).

Tides in the Red Sea are oscillatory and semidiurnal. The nodal point is at about 19° N where the tidal height is at its lowest, but it fluctuates between 20 and 30 cm away from the nodal point (Morcos 1970). Because of the small tidal range in Jeddah area, the water during high tide seeps through numerous holes to the topographic depression in the studied pans. On the other hand, south of Jeddah in the Shuiaba area, the water from the lagoon may cover the adjoining sabkhas as far as 3 km, whereas north of Jeddah in the Al-kharrar area, the sabkhas are covered by a thin sheet of water as far as 2 km. Winter mean sea level is 50 cm higher than in summer. Waves are generated by winds and tidal action. Water temperature ranges between 25.5 and 31.0 °C, but higher temperatures could be reached in the very shallow and isolated coastal areas (Edwards 1987). The same fact applies to salinity which has an average value of 39.2‰ but may exceed 40‰.

Sediment characteristics of the saline pans

Field examination of Ṣarūm area indicates that the saline pans occupy the lowest topographic depressions that are surrounded with wet supratidal sabkha, dry sandflat, and Pleistocene carbonate sediments toward the higher topographic area (Fig. 1c). The Pleistocene carbonates form a mesa that is composed of coral reefs, bivalves, and gastropods, 1–1.5 m high, and at a distance of 15–30 m from the margin of the gypsum pan (Fig. 2a). Some coral masses are standing out in the gypsum pan and are encrusted with mushroom gypsum mound (Fig. 2b). The dry sandflat area is composed of wind-blown sand-sized quartz grains, in addition to sand and gravel-sized bioclasts, coral debris, mollusk shells, and some reworked gypsum crystals (Fig. 2c). The water table in the dry sandflat exceeds 50 cm in depth. The wet, very soft, sabkha area surrounds the saline pans and contains seepage channels that are floored with green and yellow cyanobacterial mats (Fig. 2d). Groundwater is located at a depth of less than 10 cm and may enclose small (<5 m^2) and shallow (<20 cm)

Fig. 2 Dry sandflat and wet sabkha area. **a** Branching coral from the raised Pleistocene terrace facing the gypsum pan. **b** Coral heads are encrusted with gypsum and forming mushroom and domal morphologies. **c** Gastropod shells and other bioclasts form the dry sandflat area. **d** Surface seepage of seawater floored with green cyanobacteria, with beige, high area of gypsum mounds. **e** Petee structure dominates the wet, sabkha area that surrounds the halite and gypsum pans. **f** The sabkha sediments are composed of pink gypsum, overlain with green and violet cyanobacteria-rich sediments that overlay a black zone of decayed microbial mats rich in gypsum

depressions that are floored with gypsum crystals and microbial mats. In general, the sabkha area is composed of thin, buckled gypsum crusts that form elongated, polygonal ridges associated with microbial mats that form a petee structure (Fig. 2e). The peripheral, submerged part of the sabkha is usually covered with varicolored cyanobacterial mats mixed with gypsum crusts (Fig. 2f). The topmost gypsum crust consists of rosette and prismatic crystals, underlain with green cyanobacteria and dark gray, decayed subrecent microbial mat and gypsum crystals (Fig. 2f). Gypsum and microbial mats may develop into <50 cm in size, stromatolitic, single and merged gypsum domes in a brine with 15 cm depth. The brine is pinkish in color, with salinity that ranges from 80 to 175‰ and density that ranges from 1.08 to 1.12 g/cm^3.

The halite pan is surrounded with sabkha sediments toward the seaside and dry sandflat in the eastern side. Halite

crystallized in the pan at the brine-air interface as a cumulation of rafts and pyramidal hoppers (Fig. 3a) or at the floor of the pan as chevrons and cornets (Fig. 3b). The halite crystals may aggregate to form cauliflowers, mushrooms, and halite tables (Fig. 3c). Some parts of the pan show a partial dissolution of the halite crusts by low salinities, seawater seepage, and/or rainfall to form microkarst pits and pipes (Fig. 3d). Truncation surfaces are common between the halite layers (Taj and Aref 2015). Measured salinity for the brines in the halite pan exceeds 250‰, whereas the trickled seepage seawater within the pan has a salinity around 40‰.

The gypsum pan is surrounded with 3–17 m wide area of old polygonal gypsum crusts that mark the drowned level of the pan. The gypsum polygons form elongated ridges parallel or less common normal to the present shoreline of the pan (Fig. 3e). The ridges have a smooth upper surface or inverted V-shaped, sharp tepee crusts (Fig. 3f). At the shallow part of the gypsum pan, similar 10–15-cm-thick, recent, polygonal gypsum ridges (Fig. 3g) or individual domes (Fig. 2b) existed. They are composed of interbedded, 1–5-cm-thick, gypsum crusts and <5-mm-thin laminae of green to black microbial mats. The gypsum crusts are composed of fibrous and rosette gypsum crystals (Fig. 3h). The salinity of flowing seawater seepage is 80‰ and its density is 1.08 g/cm^3, in contrast to the measured values of salinity 160–180‰ and density 1.12–1.13 g/cm^3 for the brine of the gypsum pan.

Results and discussion

Chemical composition of the brines

The distribution of the concentrations of the cations Na^+, K^+, Ca^{2+}, and Mg^{2+}; the anions Cl^-, SO_4^{2-}, and HCO_3^-; TDS; and alkalinity are presented in Figs. 4 and 5. The concentrations of cations and anions are expressed in milligrams per liter. Na^+ has the highest concentration with respect to the cations K^+, Mg^{2+}, and Ca^{2+} in the halite and gypsum pans (Fig. 4a). Na^+ concentration in the halite pan is relatively higher than that found in the gypsum pan. Mg^{2+} concentration is next in abundance, followed by K^+, whereas very low concentration of Ca^{2+} is recorded in most samples (Fig. 4a). For the anions, the Cl^- concentration is the highest, SO_4^{2-} concentration is very low, whereas the HCO_3^- is the lowest (Fig. 4b). However, the concentrations of Na^+ and K^+ increase to 58, 200 and 10,800 mg/l, respectively, toward the northeastern part of the saline pans, i.e., toward the eastern part of the halite pan (Fig. 5a, b). The Na^+ and K^+ concentrations decreased toward the western and southern parts (16,000 and 500 mg/l), respectively. The low values of Na^+ concentration at the western part of the saline pans are attributed to dilution from Red Sea water and less evaporation compared to the northeastern part. Also, the low value of Na^+ concentration in the southern gypsum pan is due to low salinity of the pan (<120 ‰), in comparison to the northern halite pan (>250‰). Also, the volume of water body in the northern halite pan is much smaller than those in the southern gypsum pan. Therefore, the latter is less evaporated than the former. Because of the fact that the halite and gypsum pans are located at a distance of 1400 and 150 m, respectively, from the Red Sea coast, it is expected that the dilution from the Red Sea to the gypsum pan is much higher than that in the halite pan.

The Ca^{2+} concentration increases to 1723 mg/l toward the southern part of the saline pans (Fig. 5c). The Mg^{2+} and Cl^- (Fig. 5d, e) contents follow the same trend of Na^+ concentration, i.e., they increase to 31,567 and 209,452 mg/l toward the halite pan. The concentration of HCO_3^- increases to 732 mg/l toward the northeastern part of the gypsum pan (Fig. 5g) that coincides with a decline in SO_4^{2-} content (Fig. 5f). SO_4^{2-} reduction by bacteria may explain the increase in HCO_3^- and alkalinity and the decline in SO_4^{2-} concentration in the eastern part of the gypsum pan. The black nature of the subrecent sediments at a depth of 5 cm (Fig. 3h) and the strong smell of H_2S gas in the eastern part of the gypsum pan may confirm the reduction of SO_4^{2-} by sulfate-reducing bacteria and the liberation of H_2S gas, similar to the observations by Deng et al. (2010), Spadafora et al. (2010), and Glunk et al. (2011). Also, the increase in HCO_3^- content in the northeastern part of the halite pan results from oxidation of organic matter and reduction of SO_4^{2-}. The dominance of microbial mats in the gypsum and halite pans (Figs. 2f and 3h) may explain the high values of HCO_3^- and alkalinity and the relatively lower values of SO_4^{2-}.

The TDS concentration is highest 350,000 mg/l at the northeastern part of the halite pan (Fig. 5h). The TDS concentration is decreased to 150,380 mg/l at the western part of the halite pan (Table 1 and Fig. 5h), which is compatible with deposition of gypsum and flourishing of microbial mats and the presence of numerous seawater seepage points (Fig. 2d). In general, the TDS value of the gypsum pan is lower than that in the halite pan (Table 1). The TDS value of the gypsum pan ranges from 69,600 to 237,116 mg/l, whereas the TDS value of the halite pan ranges from 150,380 to 359,560 mg/l (Table 1). The exceptional low values of TDS in the gypsum and halite pans are observed in the areas of seawater seepage. The small surface area and the lower depth (<30 cm) of the halite pan, in comparison to the large surface area and higher depth (>150 cm) of the gypsum pan, are topographic factors that control the volume of water, evaporation, and salinities of these pans. Therefore, the higher water volume in the southern gypsum pan leads to lower TDS values. Whereas the northern halite pan is far from sea and has a lower water volume, therefore, low dilution and high evaporation rate are expected that increase the salinity of its brine.

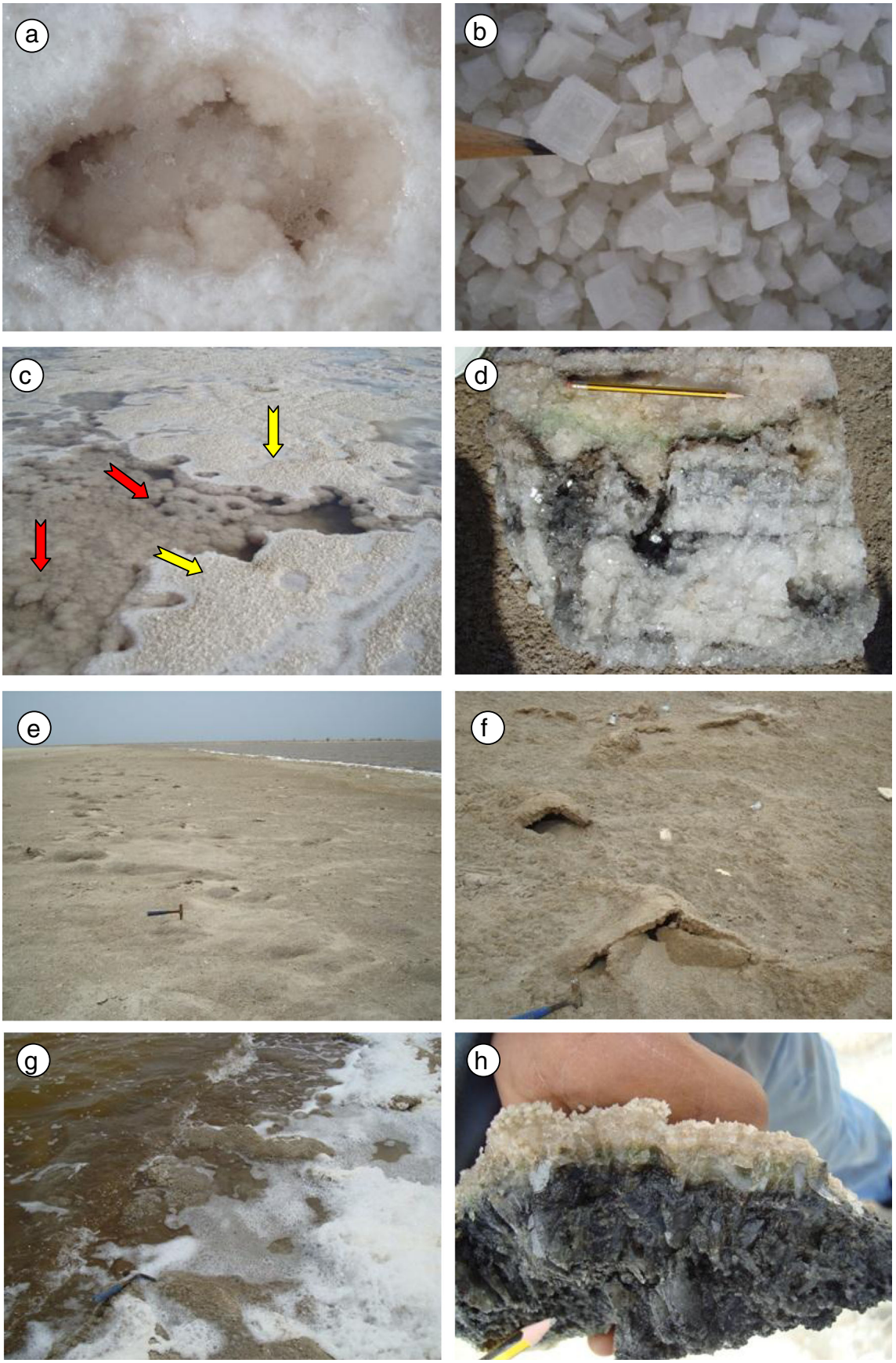
a
b
c
d
e
f
g
h

◀ **Fig. 3** Halite and gypsum pans. **a** Thin, halite raft nucleates at the brine-air interface in a small depression. **b** Halite cornets and chevrons grow at the floor of the pan. **c** Growth of halite as cauliflowers at the floor of the pan (*red arrows*), and as a table-like form near the brine surface (*yellow arrows*). **d** Microkarst pits and pipes filled with clay and cubic halite cement and cross the halite layers. **e** Polygonal gypsum ridges mark the former shoreline of the retreat shore of the gypsum pan. **f** Large polygonal tepee structure with inverted V-shaped crests. **g** Submerged, polygonal, elongated gypsum ridges form at the margin of the gypsum pan. **h** Cross section in the gypsum ridge, showing an upper white gypsum with green cyanobacteria, and a lower black gypsum dominated with decayed microbial mats

Brine types

The ionic concentrations of the brines show the following general pattern: $Na^{+}>Mg^{2+}>Ca^{2+}>K^{+}$ in sample number 1 (seawater) and sample numbers 14, 15, 16,17, 18, 19, 22, and 24 of the gypsum pan (Table 1), whereas $Na^{+}>Mg^{2+}>K^{+}>Ca^{2+}$ was the pattern in samples 12, 13, 20, 21, and 23 of the gypsum pan and samples 2, 3, 4, 5, 6, and 9 of the halite pan. In only four sample numbers—7, 8, 10, and 11—of the halite pan, the ionic concentrations of the brine samples have the following general pattern: $Mg^{2+}>Na^{+}>K^{+}>Ca^{2+}$. For the anions, the ionic concentrations in all samples of the halite and gypsum pans have the following general pattern: $Cl^{-}>SO_4^{2-}>HCO_3^{-}$. From the concentration of the major ions, five types of brines are recognized (Table 1). Most brine samples (five samples in the halite pan and eight samples in the gypsum pan) are of Mg and sodium chloride water type. Approximately, three to four samples have the following brine types: Ca, Mg, sodium chloride; or Mg, sodium, SO_4, chloride; or K, Na, magnesium chloride. Whereas only one sample from the halite pan is of Na and magnesium chloride water type.

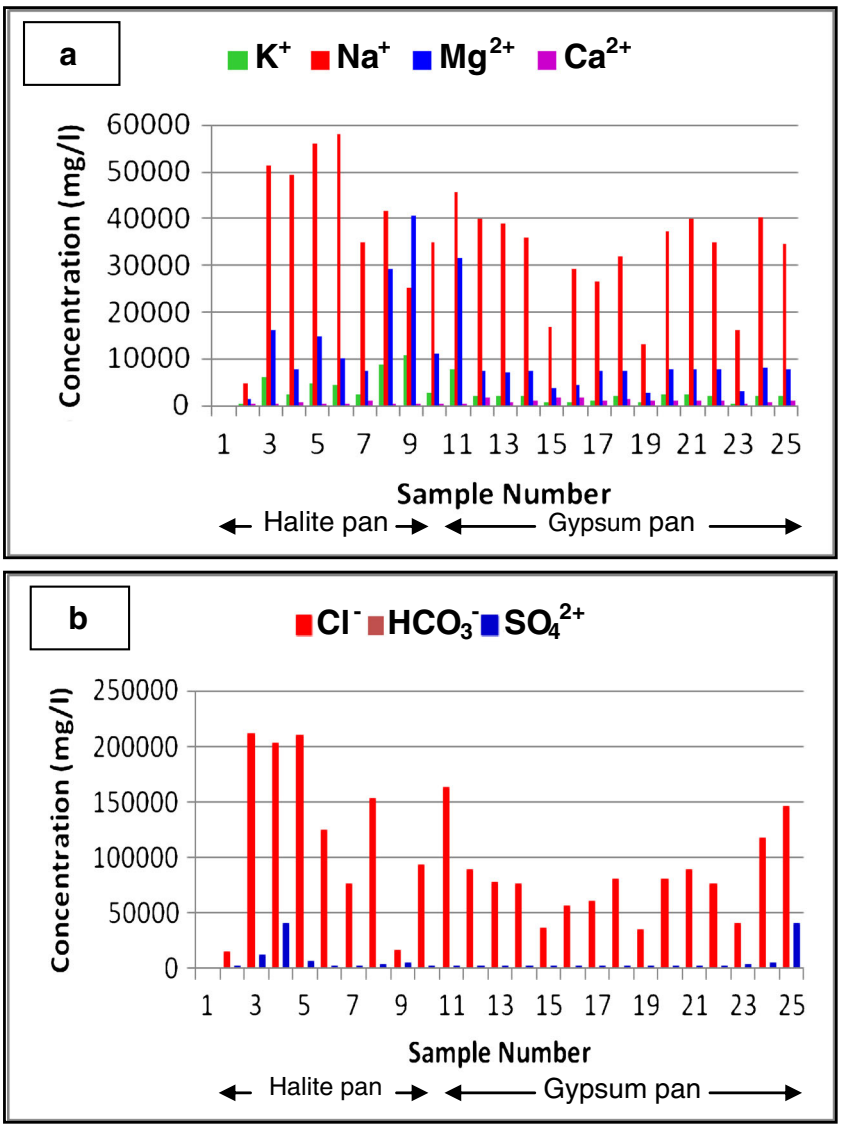

Fig. 4 **a**, **b** Concentration of the major cations and anions (mg/l) in the halite and gypsum pans, Şarūm area

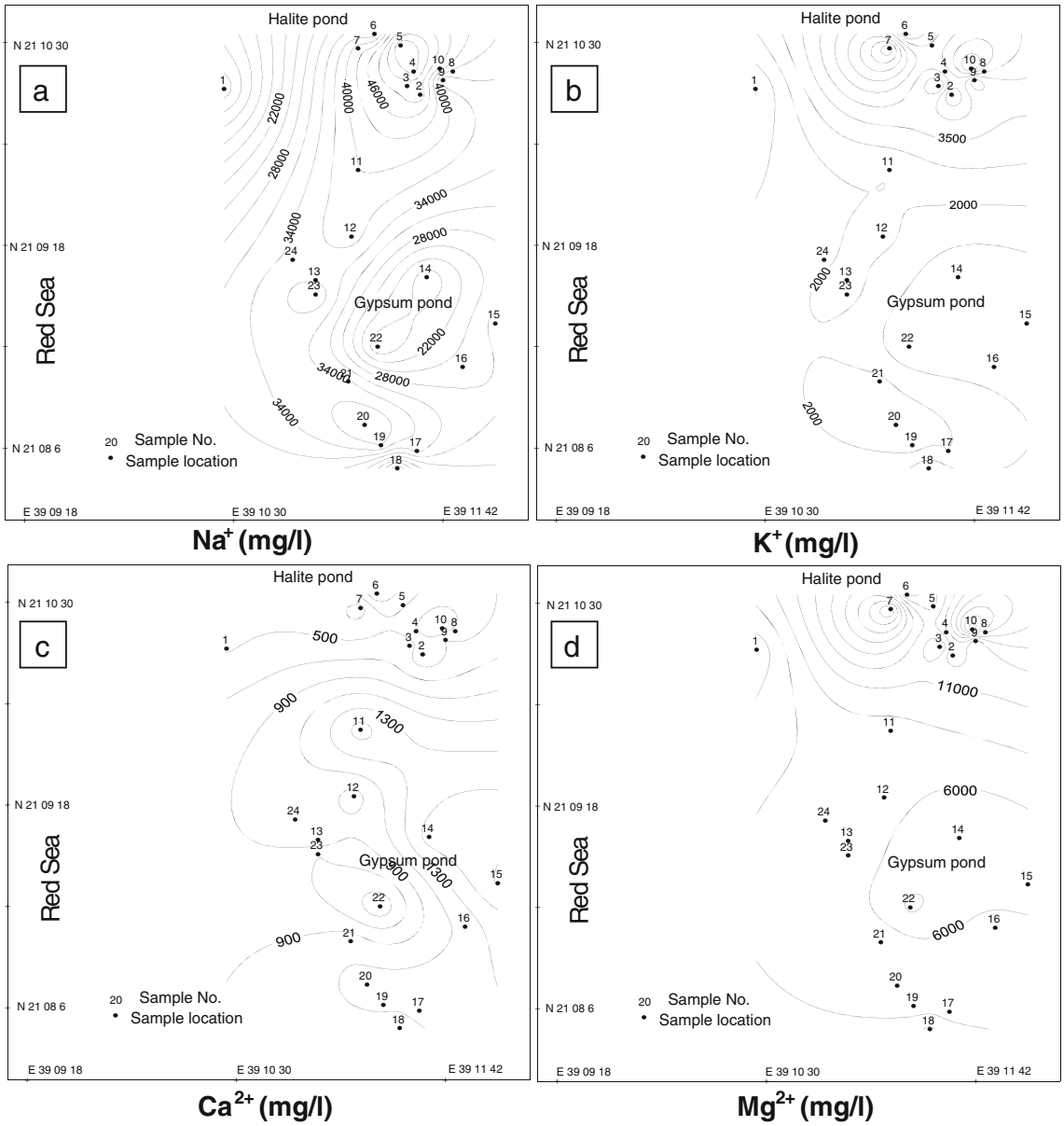

Fig. 5 **a**–**h** Distribution of the major cations and anions and alkalinity in the studied halite and gypsum pans, Ṣarūm area

Ion interrelationship

The correlation of the concentration values of cations, anions, alkalinity, and TDS is shown in Fig. 6. The correlation between Na^+ and Cl^- indicates a positive relationship (Fig. 6a), as a result of the precipitation of NaCl (halite) from the brine at high salinity. The correlation between Ca^{2+} and Mg^{2+} indicates a negative relationship (Fig. 6b). The depletion of the brines in Ca^{2+} is due to precipitation of $CaCO_3$ (calcite and aragonite) and $CaSO_4{\cdot}2H_2O$ (gypsum). No pronounced relationship is observed between Ca^{2+} and SO_4^{2-}, despite of the common precipitation of gypsum in the saline pans (Fig. 6c). Most probably, the reduction of SO_4^{2-} by sulfate-reducing bacteria leads to further removal of the SO_4^{2-} from the brine, similar to the observation by Deng et al. (2010), Spadafora et al. (2010), and Glunk et al. (2011). The same interpretation may be applied to the negative correlation between Ca^{2+} and HCO_3^- (Fig. 6d), where oxidation of organic matter and reduction of sulfate ions lead to the increase in HCO_3^- and alkalinity. The positive relationship between HCO_3^- and alkalinity confirms the role of sulfate-reducing bacteria in the oxidation of organic matter and the increase of HCO_3^- and alkalinity (Fig. 6e). There is a strong positive relationship between TDS and Cl^- (Fig. 6f) and between TDS and Na^+ (Fig. 6g) and a very strong relation between TDS and SO_4^{2-} (Fig. 6h). These positive

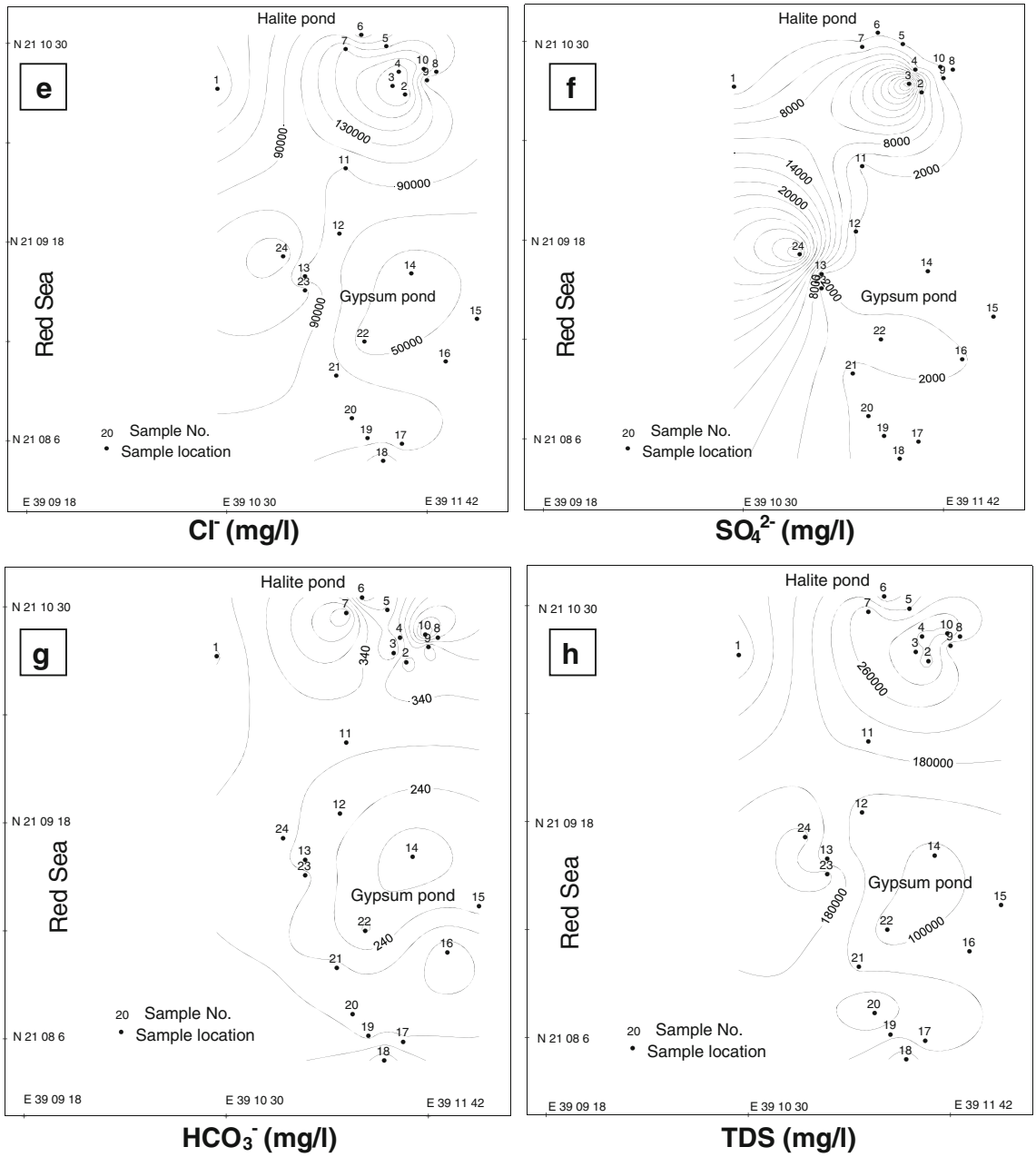

Fig. 5 (continued)

relationships indicate that the TDS are mainly represented by chloride and sulfate ions.

The ratio Mg/Ca with respect to sample numbers and TDS are shown in Fig. 7. It is clear that Mg/Ca is greatly higher in the halite pan than that recorded in the gypsum pan (Fig. 7a, b). The Mg/Ca ranges from 3.1 to 406.67 in the halite pan and 3.17 to 11.48 in the gypsum pan (Table 1). The exceptional very high Mg value in the halite pan is accompanying the very high salinity of 375,023 mg/l which indicates that the brine reaches the evaporation stage that will precipitate the bittern salts $MgCl_2$ and KCl minerals. The relatively high Mg/Ca in the gypsum and halite pans allows the dolomitization of the early calcite and aragonite crystals.

Brine evolution

The evolution of the brine of the Şarūm pans can be understood using the analytical data obtained from brine samples as a result of plotting the major cations and anions in the Piper trilinear diagrams (Fig. 8a, b). The diagrams show that the majority of brine samples of the halite pan are located in the field NaCl type of water. Some samples fall in the MgNaCl-type facies. Also, from the Piper plot, the alkali metals (Na^+ +

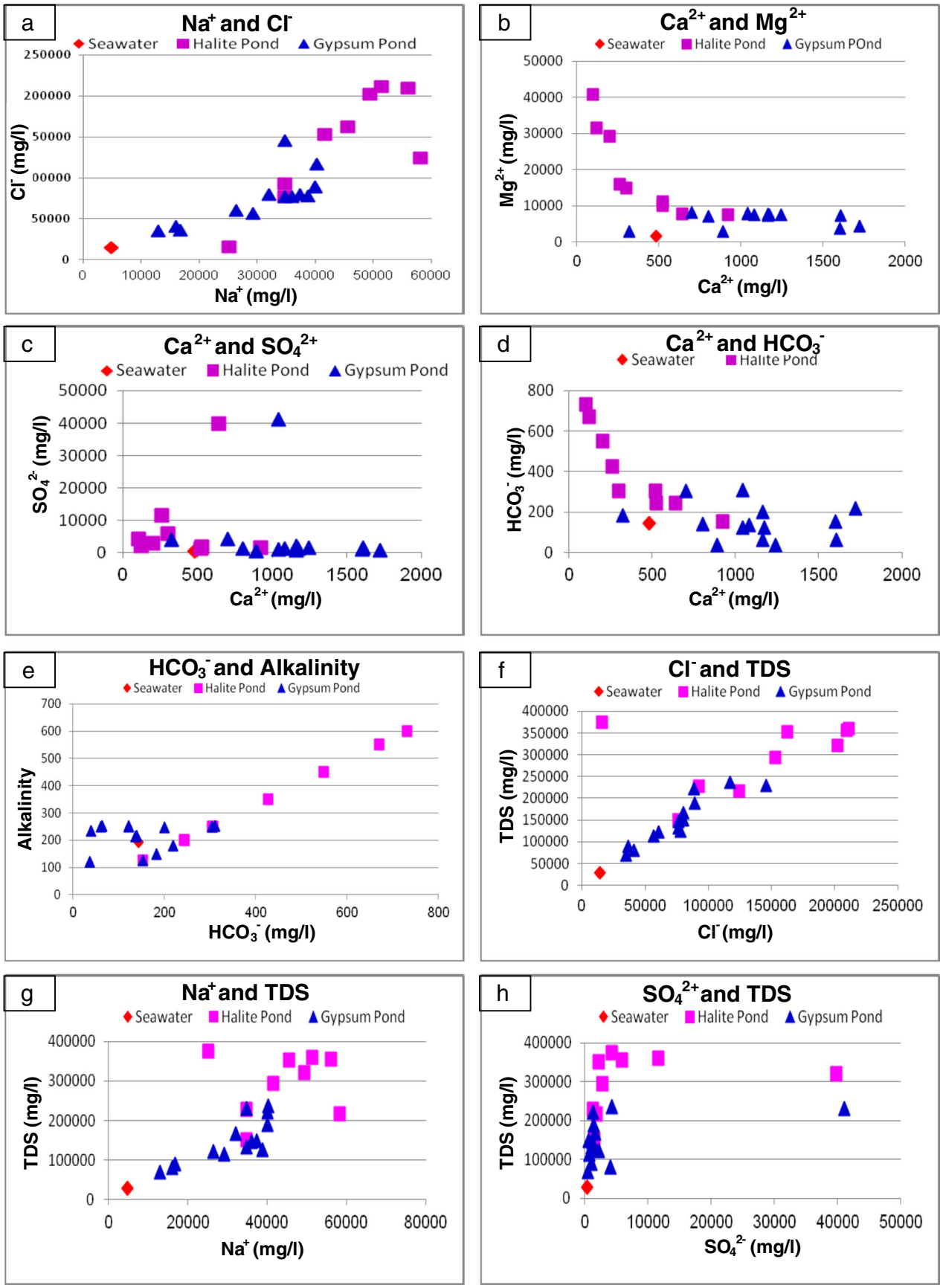

Fig. 6 **a**–**h** Relationships between various anions, cations, alkalinity, and TDS

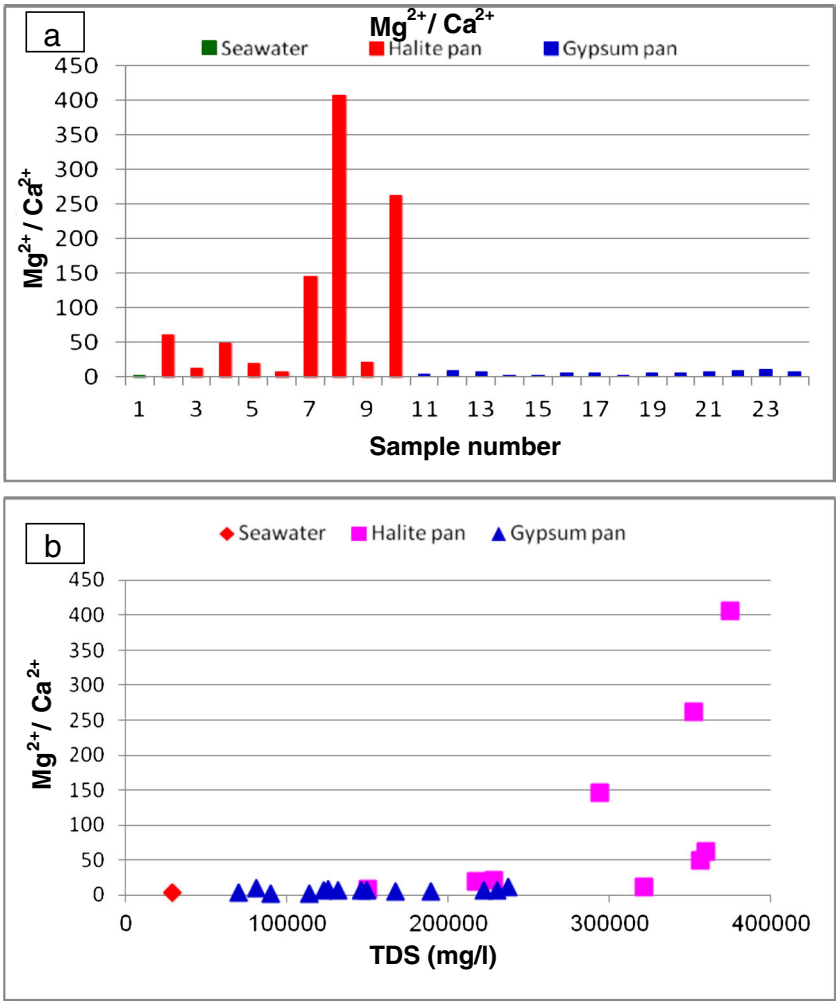

Fig. 7 Relationship between Mg/Ca and sample number (**a**) and TDS (**b**)

K^+), and the alkaline earth element Mg^{2+} significantly exceeds the alkaline earth element Ca^{2+}, whereas the strong acid (Cl^-) greatly exceeds the weak acids (HCO_3^- and CO_3^{2-}) and the strong acid (SO_4^{2-}).

On the other hand, the Piper trilinear diagrams show that all brine samples of the gypsum pan that have different salinities are located in the field NaCl type of water. It appeared that all brine samples in the gypsum pan have similar affinity and composition that are similar to the composition of seawater. The deficiency of Ca^{2+} in the brines of the halite and gypsum pans is due to its precipitation as calcite, aragonite, and gypsum. The high value of Mg^{2+} may be precipitated as bittern salts in extreme high evaporation and low humidity and also leads to dolomitization of the early precipitated carbonate minerals.

Despite of the occasional rainfall in Jeddah area and its surroundings, the chemical composition of the brine in the studied saline pans is different from the chemical values of the rainfall in Wadi Fatimah, east of Jeddah. On the other hand, the chemical composition of the studied brine is similar to the chemical composition of seawater as shown in the Piper diagrams (Fig. 8). The chemical composition of rainwater in Wadi Fatima has the following ionic concentration pattern: $Ca^{2+}>Na^+>Mg^{2+}$ and $HCO_3^->SO_4^{2-}>Cl^-$ (Alyamani and Hussein 1995). Ca^{2+} and HCO_3^- are the dominant ions, indicating that the rainwater character is of Ca^{2+} $(HCO_3)_2$ water type (Sharaf 2013). The ionic concentration pattern of seawater in Şarūm area is as follows: $Na^+>Mg^{2+}>Ca^{2+}>K^+$ and $Cl^->SO_4^{2-}>HCO_3^-$, which is nearly the same as the concentration pattern of most samples. Therefore, the chemical characters of the studied brines and seawater are similar, and they are completely different with the chemical character of rainwater. It is worth mentioning that the brine chemistry has been modified and tends to reflect the chemical evolution from the initial calcium carbonate and calcium sulfate deposition to sodium chloride-dominant composition.

Genesis of the brines

Results of the chemical analyses were recalculated for both the major cations and anions and plotted on Sulin graph (Fig. 9), for interpretation of the origin of brine. It is clear that most of the brine samples are located near the division line between

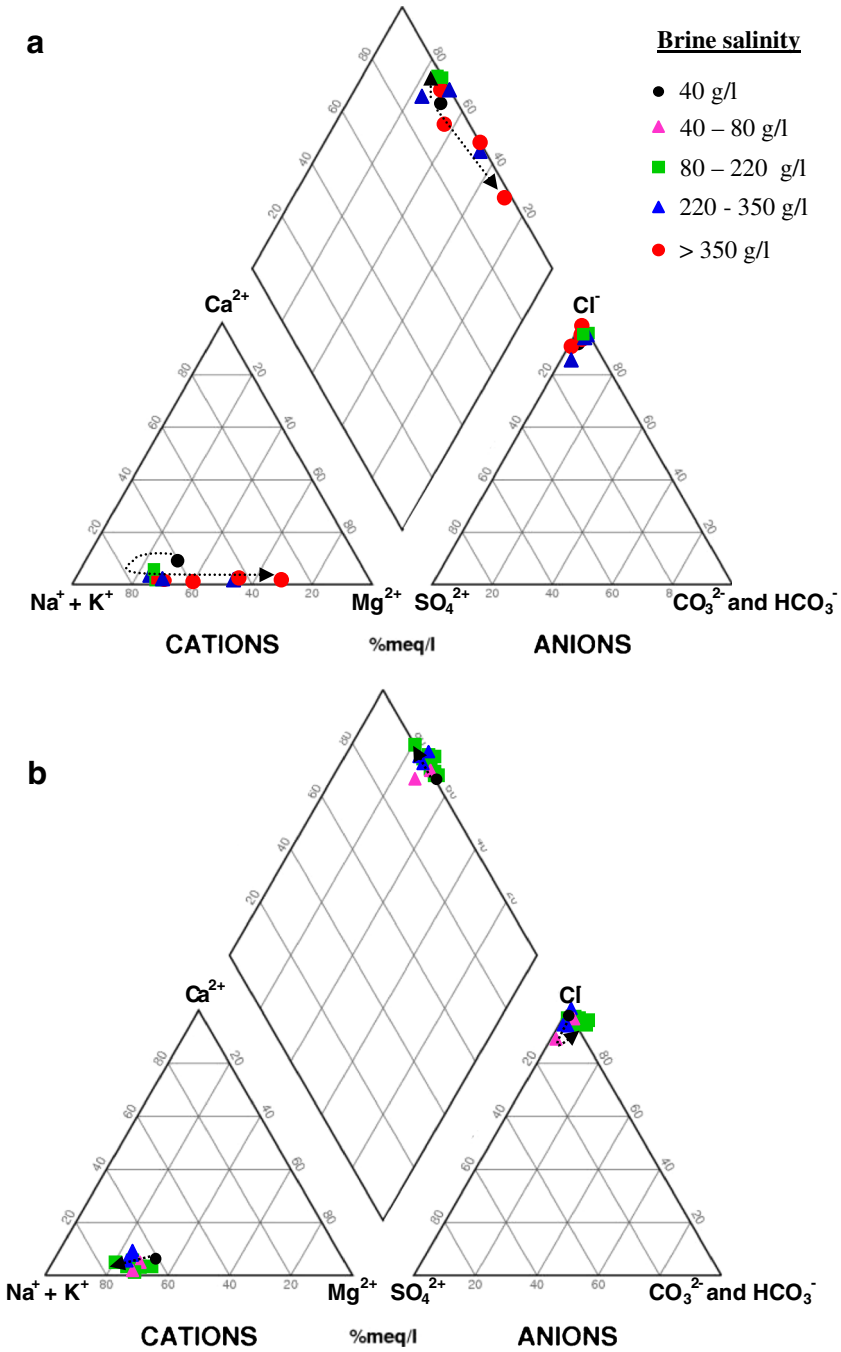

Fig. 8 Piper trilinear diagrams showing the brine evolution of the halite pan (**a**) and gypsum pan (**b**), Ṣarūm area

recent marine water and old marine water. All brine samples from the halite pan are located in the old marine water origin and of $CaCl_2$ composition. Also, most of the brine samples of the gypsum pan are located in the recent marine water origin and of $MgCl_2$ composition (Fig. 9). Therefore, the main supply to the saline pans is through seawater seepage. The $CaCl_2$ nature of the brine of some brine samples may be related to reaction of the seawater seepage with beach carbonate sediments. The contribution of freshwater through Wadi Fatima or occasional rainfall has a minor effect on the composition of the brine in the saline pans.

Conclusions

Sediment distribution in the saline pans and surrounding wet, sabkha areas reflects the salinity and chemical characteristics of the brines. Despite of the same climatic factors of evaporation rate, rainfall, humidity, and wind speed over the pans, their salinity levels fluctuated widely according to the amount of seawater seepages, brine depth, surface area of the pans, and their relative distance from the Red Sea shoreline. The saline pans and wet sabkha areas contained seawater seeps that continually supplied salts without introducing sufficient

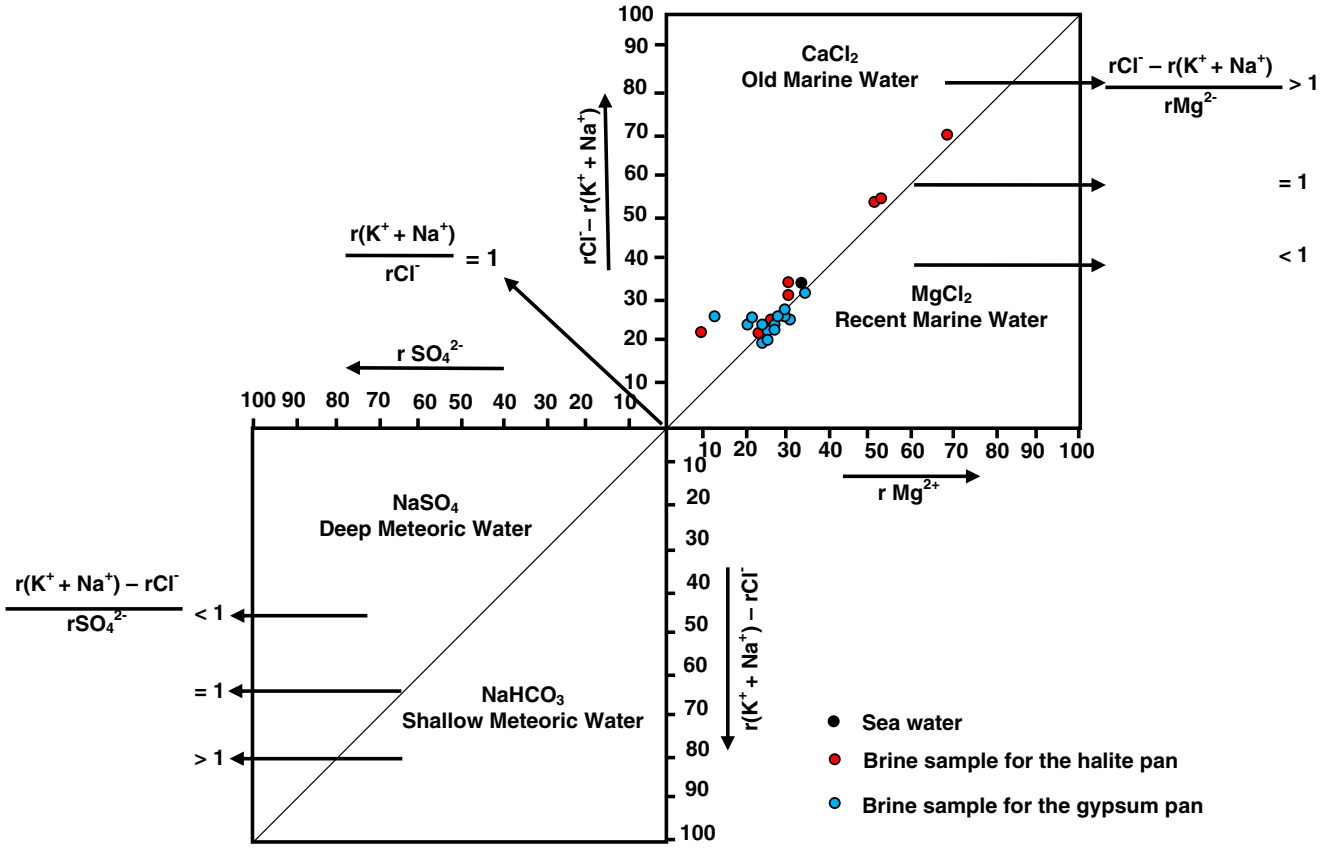

Fig. 9 Sulin graph showing the origin and type of the brine, Ṣarūm area

seawater to cause flushing. Contemporaneous formation of microbial mats and deposition of gypsum and/or halite in the gypsum and halite pans were controlled primarily by the salinity of the depositing brines. Microbial mats dominate the wet sabkha area at the western margin of the halite pan and most parts of the gypsum pan at a salinity value below 80‰. Gypsum crystallized in areas with salinity that ranges from 80 to 140‰. These salinity values were recorded in the sabkha brines at the western margin of the halite pan and in most brines of the gypsum pan. The increases of the salinity to 220‰ at the western part of the halite pan to 375‰ in its eastern side favor dominant halite deposition.

Concomitant with the increases in salinity is the increase of Na^+, K^+, Mg^{2+}, and Cl^- and the decrease of Ca^{2+}, HCO_3^-, and SO_4^{2-} in the residual brines of the saline pans. These are due to the removal of Ca^{2+}, HCO_3^-, and SO_4^{2-} ions from the brines due to the precipitation of calcite, aragonite, and gypsum. The remaining brines are still oversaturated with Na^+ (+ K^+) and Cl^- ions which favor additional halite deposition. The low value of SO_4^{2-} and the relatively high values of HCO_3^- and alkalinity are most probably related to the role of sulfate-reducing bacteria which led to the reduction of SO_4^{2-} and oxidation of organic matter. The very high values of Mg^{2+} are most probably related to the formation of $MgCl_2$ brine at the extreme high evaporation of the eastern part of the halite pan. The order of cation dominance in most samples is $Na^+ > Mg^{2+} > Ca^{2+} > K^+$ and $Na^+ > Mg^{2+} > K^+ > Ca^{2+}$. Few brine samples in the halite pan have $Mg^{2+} > Na^+ > K^+ > Ca^{2+}$. The anion dominance for all samples is $Cl^- > SO_4^{2-} > HCO_3^-$. The dominant brine type is Mg and sodium chloride, in addition to minor types of Ca, Mg, sodium chloride; or Mg, sodium, SO_4, chloride; or K, Na, magnesium chloride. These brine types indicate the dominant sodium chloride composition with variable amounts of the ions Ca^{2+}, K^+, and Mg^{2+}.

The brines of the saline pans have evolved from seawater seepage rather than from direct rainfall, or inflow from shallow aquifer. Based on the hydrochemical characteristics of the brines, the order of the dominance of cations and anions, and the presence of seawater seepage points of similar salinity to the Red Sea water (40‰), it is concluded that the brines of the saline pans have evolved from the Red Sea water through successive evaporation stages during formation of microbial mats and deposition of gypsum and halite in the extremely high evaporation status. Comparison of the sediment distribution and brine chemistry of the gypsum and halite pans is useful for the interpretation of similar ancient evaporite deposits formed in coastal, saline pans.

Acknowledgments This project was funded by the Deanship of Scientific Research (DSR), King Abdulaziz University, Jeddah, under grant

No. 289 / 145 / 1432. The authors, therefore, acknowledge with thanks the technical and financial support of DSR. Thanks are also extended to the anonymous reviewers for their careful reading of the manuscript and their valuable comments.

References

Al-Ahmadi ME (2013) Groundwater quality assessment in Wadi Fayd, Western Saudi Arabia. Arab J Geosci 6:247–258

Al-Barakati AMA (2009) Water exchange of Sharm Obhur, Jeddah, Red Sea. J K A U Mar Sci 20:49–58

Al-Barakati AMA (2011) A hydrographic study of Ras Hatiba Lagoon, Red Sea. Int J Eng Technol IJET-IJENS 11:48–64

Al-Harbi O, Hussain G, Khan MM (2010) Hydrogeochemical processes and isotopic characteristics of inland sabkha, Saudi Arabia. Asian J Earth Sci 3(1):35–49

Alsaaran NA (2008) Origin and geochemical reaction paths of sabkha brines: Sabkha Jayb Uwayyid, eastern Saudi Arabia. Arab J Geosci 1:63–74

Al-Sayari SS, Zotl JG (1978) Quaternary period in Saudi Arabia, V.I. Springer-Verlag, Wein, 335 p

Al-Shaibani A (2013) Economic potential of brines of Sabkha Jayb Uwayyid, Eastern Saudi Arabia. Arab J Geosci 6:2607–2618

Al-Subhi AM (2012) Estimation of evaporation rates in the southern Red Sea based on the AVHRR sea surface temperature data. J K A U Mar Sci 23(1):77–89

Al-Washmi HA (1999) Sedimentological aspects and environmental conditions recognized from the bottom sediments of Al-Kharrar Lagoon, Eastern Red Sea coastal plain, Saudi Arabia. J K A U Mar Sci 10:71–87

Al-Washmi HA (2003) Sediment distribution pattern in the Al-Shuaiba Lagoon, Red Sea coast of Saudi Arabia. Qatar Univ Sci J 23:5–22

Alyamani MS (1999) Physio-chemical processes on groundwater chemistry, under arid climatic conditions, western province, Saudi Arabia. Project No. 203/418. King Abdulaziz Uni, Jeddah

Alyamani MS (2007) Effects of cesspool system on groundwater quality of shallow bedrock aquifers in the recharge area of Wadi Fatimah, Western Arabian Shield, Saudi Arabia. J Environ Hydrol 15, paper 8

Alyamani MS, Hussein MT (1995) Hydrochemical study of groundwater in recharge area, Wade Fatimah basin, Saudi Arabia. Geol J 37(1): 81–89

Alyamani MS, Bazuhair AS, Bayumi TH, Al-Sulaiman K (1996) Application of environmental isotope on groundwater study in the western province, Saudi Arabia. Project No. 005/413. King Abdulaziz University, Jeddah

APHA (American Public Health Association) (2005) Standard methods for the examination of water and wastewater, 20th edn. APHA-AWWA-WET, Washington

Bahafzallah AAK, El-Askary MA (1981) Sedimentological and micropaleontological investigations of the beach sands around Jeddah, Saudi Arabia. J K A U Earth Sci 4:25–42

Bahafzullah AAK, Fayed LA, Kazi A, Al-Saify M (1993) Classification and distribution of the Red Sea coastal sabkha near Jeddah, Saudi Arabia. Carbonates Evaporites 8:23–38

Banat KM, Howari FM, Kadi KA (2005) Water chemical characteristics of the Red Sea coastal sabkhas and associate evaporite and carbonate minerals. J Coast Res 21(5):1068–1081

Basaham AS (1998) Distribution and behavior of some heavy metals in the surface sediments of Al-Arbaeen lagoon, Jeddah, Red Sea coast. J K A U Earth Sci 10:59–71

Basyoni MH (1997) Sedimentological and hydrochemical characteristics of Al-Lith sabkha, Saudi Arabia. J K A U Earth Sci 9:75–86

Basyoni MH, Mousa BM (2009) Sediment characteristics, brine chemistry and evolution of Murayr Sabkha, Arabian (Persian) Gulf, Saudi Arabia. Arab J Sci Eng 34(2A):95–123

Deng S, Dong H, Lv G, Jiang H, Yu B, Bishop ME (2010) Microbial dolomite precipitation using sulfate reducing and halophilic bacteria: results from Qinghai Lake, Tibetan Plateau, NW China. Chem Geol 278:151–159

Edwards AJ (1987) Climate and oceanography. In: Edwards AJ, Head SM (eds) Red Sea. Pergamon Press, Oxford, pp 45–69

El Sayed MA (2002) Nitrogen and phosphorus in the effluent of a sewage treatment station on the eastern Red Sea coast: daily cycle, flux and impact on the coastal area. Int J Environ Stud 59:73–94

El-Rayis OA, Moammar MO (1998) Environmental conditions of two Red Sea coastal lagoons in Jeddah. 1. Hydrochemistry. J K A U Mar Sci 9:31–47

El-Sabrouti MA (1983) Texture and mineralogy of the surface sediments of Sharm Obhur, West Red Sea Coast of Saudi Arabia. Mar Geol 53: 103–116

Glunk C, Dupraz C, Braissant O, Gallagher KL, Verrecchia EP, Visscher PT (2011) Microbially mediated carbonate precipitation in a hypersaline lake, Big Pond (Eleuthera, Bahamas). Sedimentology 58: 720–738

Herczeg AL, Dogramaci SS, Leaney FW (2001) Origin of dissolved salts in a large, semi-arid groundwater system: Murray Basin. Mar Freshw Res 52:41–52

Lowenstein TK, Hardie LA (1985) Criteria for the recognition of salt-pan evaporites. Sedimentology 32:627–644

Macumber PG (1991) Interaction between groundwater and surface systems in northern Victoria. Victoria Department of Conservation and Environment, Melbourne, 345 pp

Mandurah MH, Aref MAM (2012) Lithostratigraphy and standard microfacies types of the Neogene carbonates of Rabigh and Ubhur areas, Red Sea coastal plain of Saudi Arabia. Arab J Geosci 5:1317–1332

MAW (Ministry of Agriculture and Water) (2003) Yearly report on agriculture and water, 2002, Kingdom of Saudi Arabia. Kingdom of Saudi Arabia, Riyadh

Moore TA, Al-Rehaili MHA (1989) Geologic map of the Makkah Quadrangle, sheet 21D, Kingdom of Saudi Arabia. Ministry of Petroleum and Mineral Resources, Jeddah

Morcos SA (1970) Physical and chemical oceanography of the Red Sea. Oceanogr Mar Biol Annu Rev 8:73–202

Patzert WC (1974) Wind-induced reversal in Red Sea circulation. Deep-Sea Res 21:109–121

Qari MHT (2009) Geomorphology of Jeddah Governorate, with emphasis on drainage systems. J K A U Earth Sci 20(1):93–116

Radke LC, Howard KWF (2007) Influence of groundwater on the evaporative evolution of saline lakes in the Wimmera of south-eastern Australia. Hydrobiologia 591:185–205

Radke LC, Howard KWF, Gell PA (2002) Chemical diversity in south-eastern Australian Lakes I: geochemical causes. Mar Freshw Res 53: 941–959

Sabtan AA, Shehata WM (2003) Hydrogeology of Al-Lith Sabkha, Saudi Arabia. J Asian Earth Sci 21:423–429

Sabtan AA, Shehata WM, El-Mahdy OR (1997) Assessment of economic potentialities of sabkhah brines, Western Region, Saudi Arabia. Technical report submitted to King Abdulaziz University, Project No. 415/138, 221 pp

Sharaf MAM (2013) Major elements hydrochemistry and groundwater quality of Wadi Fatimah, West Central Arabian Shield, Saudi Arabia. Arab J Geosci 6:2633–2653

Skipwith P (1973) The Red Sea and coastal plain of the Kingdom of Saudi Arabia, Saudi Arabian Directorate General of Mineral Resources, Technical Record TR-1973-1, 149 pp

Spadafora A, Perri E, Mckenzie J, Vasconcelos C (2010) Microbial biomineralization processes forming modern Ca:Mg carbonate stromatolites. Sedimentology 57:27–40

Spencer CH, Vincent PL (1984) Bentonite resources potential and geology of Cenozoic sediments, Jeddah region. Saudi Arabia Deputy Ministry for Mineral Resources, Open File Report BRGM-OF-04-31, 60 pp

Taj R, Aref MA (2015) Structural and textural characteristics of surface halite crusts of a supratidal, ephemeral halite pan, South Jeddah, Red Sea Coast, Saudi Arabia. Facies. doi:10.1007/s10347-014-0426-0

Turki AJ (2007) Metal speciation (Cd, Cu, Pb and Zn) in sediments from Al Shabab Lagoon, Jeddah, Saudi Arabia. J K A U Mar Sci 18:191–210

Turki AJ, Mudarris MSA (2008) Bacteria and nutrients as pollution indicators in the Al-Nawrus recreational lagoon, Jeddah. J K A U Mar Sci 19:77–93